Editors' Suggestion | Featured in Physics

$\mathcal{PT}$-symmetric circuit QED

Fernando Quijandría,[1] Uta Naether,[2] Sahin K. Özdemir,[3] Franco Nori,[4,5] and David Zueco[2,6]

[1]*Microtechnology and Nanoscience, MC2, Chalmers University of Technology, SE-412 96 Göteborg, Sweden*

[2]*Instituto de Ciencia de Materiales de Aragon and Departamento de Fisica de la Materia Condensada, CSIC-Universidad de Zaragoza, E-50012 Zaragoza, Spain*

[3]*Department of Engineering Science and Mechanics, The Pennsylvania State University, University Park, Pennsylvania 16802, USA*

[4]*Theoretical Quantum Physics Laboratory, RIKEN Cluster for Pioneering Research, Wako, Saitama 351-0198, Japan*

[5]*Department of Physics, University of Michigan, Ann Arbor, Michigan 48109-1040, USA*

[6]*Fundacion ARAID, Paseo Maria Agustin 36, E-50004 Zaragoza, Spain*

(Received 19 February 2018; published 30 May 2018)

A parity-time ($\mathcal{PT}$)-symmetric system emerging from a quantum dynamics is highly desirable in order to understand the possible implications of $\mathcal{PT}$ symmetry in the next generation of quantum technologies. In this work, we address this need by proposing and studying a circuit-QED architecture that consists of two coupled resonators and two qubits (each coupled to one resonator). By means of external driving fields on the qubits, we are able to tune gains and losses in the resonators. Starting with the quantum dynamics of this system, we show the emergence of the $\mathcal{PT}$ symmetry via the selection of both driving amplitudes and frequencies. We engineer the system such that a non-number-conserving dipole-dipole interaction emerges, introducing an instability at large coupling strengths. The $\mathcal{PT}$ symmetry and its breaking, as well as the predicted instability in this circuit-QED system, can be observed in a transmission experiment.

DOI: 10.1103/PhysRevA.97.053846

I. INTRODUCTION

One of the mathematical axioms of quantum mechanics is that the Hamiltonian H of a system should be Hermitian, i.e., $H = H^\dagger$. This axiom ensures real energy eigenvalues and, correspondingly, a unitary time evolution, for which the probability to find the system at some state is conserved. Physical systems described by Hermitian Hamiltonians represent closed systems. However, physical systems in general are open and they are in continuous energy exchange with other systems, experiencing dissipation (or absorption, loss) or receiving energy (gain) from a source. Such systems with gain or loss are described by non-Hermitian Hamiltonians, i.e., $H \neq H^\dagger$, for which the probability, in general, is not conserved and its time evolution is not unitary. It is worth pointing out here that open systems at zero temperature can *effectively* be described by non-Hermitian Hamiltonians.

In 1998, it was shown [1], however, that Hermiticity is not a necessary condition for H to have real eigenvalues. In fact, a whole class of Hamiltonians can have real eigenvalues without being Hermitian, if they are $\mathcal{PT}$ symmetric in the sense that they commute with the $\mathcal{PT}$ operator, i.e., $[\mathcal{PT}, H] = 0$, where $\mathcal{P}$ is the unitary parity operator and $\mathcal{T}$ is the antiunitary time-reversal operator [2]. It is now understood that one can interpret $\mathcal{PT}$-symmetric systems as nonisolated physical systems having balanced absorption (loss) and amplification (gain). Remarkably, such systems exhibit a phase transition—spontaneous $\mathcal{PT}$-symmetry breaking—at an exceptional point (EP), where both the eigenvalues and the corresponding eigenstates of the system coalesce, if the parameter that controls the degree of non-Hermiticity exceeds a critical value. Beyond this critical threshold, the spectrum is no longer real, and eigenvalues become complex even though $[\mathcal{PT}, H] = 0$ is still satisfied. In other words, the system experiences a *real-to-complex spectral phase transition*.

The presence of an EP (or a $\mathcal{PT}$ phase transition) drastically affects the dynamics of the system leading to counterintuitive features which can help to control wave transport and light-matter interactions. Thus, the field surrounding the concepts of $\mathcal{PT}$ symmetry and EPs (that started as a purely mathematical concept) has turned into a rapidly growing field with many interesting experiments [3–22], most of them in the field of optics. Among the nontrivial phenomena observed in these experiments are unidirectional invisibility in fiber networks [8], nonreciprocal light transport in whispering gallery microresonators [7], single-mode lasing in otherwise multimoded lasers with $\mathcal{PT}$ symmetry [23,24], loss-induced lasing [6], control of emission direction of lasing in microring lasers [9], a mobility edge in disordered optical waveguide arrays [25,26], as well as chiral dynamics [16] and topological energy transfer when encircling an EP [19]. Recent years have also seen a number of very interesting theoretical proposals revealing how $\mathcal{PT}$ symmetry can be used to enhance and control optomechanical interactions, and how $\mathcal{PT}$ symmetry affects quantum phase transitions and information retrieval in quantum systems [27–29]. For example, the works of Jing *et al.* with optomechanical microresonators have revealed the possibility of thresholdless phonon lasing [30], group velocity control via optomechanically induced transparency [31], enhanced optomechanical cooling at high-order exceptional points [32], as well as phonon analog of loss-induced lasing in optomechanical systems with two-level system defects [33]. Another interesting phenomenon, the jamming anomaly or the anomalous transport in the large gain-loss regime, has

also been studied [34]. The above-mentioned theoretical and experimental works are just a few examples showing the enormous and growing interest in $\mathcal{PT}$-symmetric systems and their realizations.

In the reported experimental works on $\mathcal{PT}$ symmetry and EPs, open classical systems are engineered such that the dynamics for the variables of interest obey the $\mathcal{PT}$ symmetry. A study of $\mathcal{PT}$ symmetry and its breaking in experimentally accessible quantum systems is highly desirable to understand the pros and cons of $\mathcal{PT}$ symmetry for developing quantum technologies. In this work, we address this need by proposing a circuit-QED architecture—a superconducting circuit operating in the quantum limit [35–40]. Starting with a microscopic and unitary description, we demonstrate that the dynamics of this circuit-QED system can be described by an *effective* non-Hermitian $\mathcal{PT}$-symmetric Hamiltonian.

The proposed circuit-QED architecture is experimentally accessible because the main ingredients, a tunable coupling between resonators [41] as well as tunability of a qubit gap [42–47], have already been experimentally demonstrated and are readily available. A circuit-QED architecture for studying $\mathcal{PT}$ symmetry will not only bring the field into the quantum realm, but will also offer numerous advantages. For example, so far all $\mathcal{PT}$-symmetry experiments (except Ref. [18]) involve two components, one with loss and the other with gain. These systems are not scalable and thus it is very difficult to expand them to a larger number of components in order to study collective behavior or the effect of global and local $\mathcal{PT}$ symmetries on wave transport and light-matter interactions. Circuit-QED architectures with their scalability (e.g., fabricating arrays of $\mathcal{PT}$-symmetric resonators and coupled qubits with a small footprint should not be a big challenge with current state-of-the-art technologies) and versatility (e.g., engineering different Hamiltonians by tuning the strength and the frequency of external drives is a natural scenario in circuit-QED) will help to overcome such shortcomings and fabrication difficulties of current platforms used in $\mathcal{PT}$ experiments. Moreover, circuit-QED provides flexibility to explore different parameter regimes which are difficult to reach in current $\mathcal{PT}$ platforms, for instance, the ultra- and deep-strong-coupling regimes in resonator-qubit interactions.

This paper is organized as follows. In Sec. II, we introduce the circuit-QED platform that we propose for the realization of $\mathcal{PT}$ symmetry and its breaking. In Sec. III, we show how one can engineer interactions that either conserve or do not conserve the number of excitations. In Secs. IV and V, we derive the effective $\mathcal{PT}$-symmetric Hamiltonian for the system and study its dynamics in the exact and broken $\mathcal{PT}$ phases. In Sec. VI, we discuss how one can probe the behavior of this circuit-QED platform in the exact and broken $\mathcal{PT}$ phases by transmission experiments. We conclude the manuscript in Sec. VII by giving a summary of our findings and future prospects. The manuscript is also accompanied by Appendices A and B where details of the derivations are provided.

II. THE CIRCUIT

The circuit-QED architecture we propose for studying $\mathcal{PT}$ symmetry is sketched in Fig. 1. It consists of two coupled

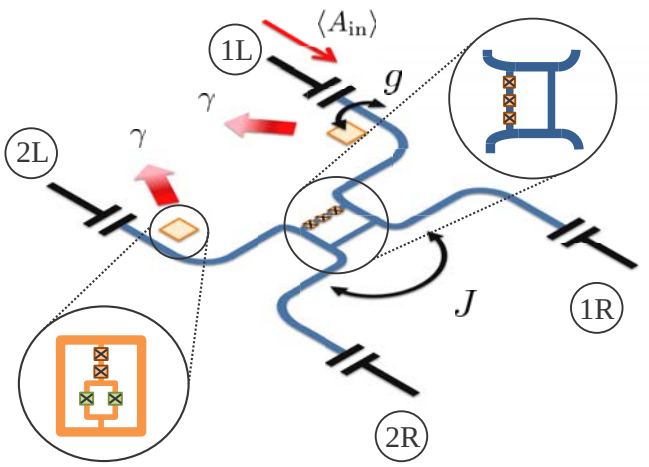

FIG. 1. A graphical illustration of the proposed circuit-QED architecture to study the physics of $\mathcal{PT}$ symmetry. Two superconductor resonators are coupled to each other with a coupling strength J, and two qubits with decay rates of γ, each coupled to one resonator with a coupling strength g, form the basic ingredients of this architecture. The inset in orange shows the structure of the qubits, whereas the inset in blue shows a possible implementation of tunable coupling between the resonators.

resonators (blue in the figure) whose coupling can be tuned over time. An experimental demonstration of a tunable coupling through a three-junction loop (sketched in the center of Fig. 1 and zoomed in the right top corner) was recently reported [41,48]. Each resonator is coupled to one qubit (orange boxes in Fig. 1) that has a tunable gap (e.g., flux qubits [44,45] or capacitively shunted qubits [46,47]). The system is described by the Hamiltonian

$$H(t) = H_0(t) + H_c(t), \tag{1}$$

where

$$H_0(t) = \sum_{j=1,2} \omega_j a_j^\dagger a_j + \frac{\epsilon_j(t)}{2}\sigma_j^z \tag{2}$$

represents the free part of the Hamiltonian. Here, ω_j are the bare frequencies of the resonators and $\epsilon_j(t)$ represent the qubit gaps that can be tuned in time. These building blocks are coupled via the interaction Hamiltonian

$$H_c(t) = \sum_{j=1,2} g_j\sigma_j^x(a_j + a_j^\dagger) + J(t)(a_1^\dagger + a_1)(a_2^\dagger + a_2), \tag{3}$$

with coupling strengths g_j and $J(t)$. The time tunability of the gaps $\epsilon_j(t)$ and the resonator-resonator coupling $J(t)$ becomes crucial in what follows.

Apart from the unitary evolution governed by $H(t)$, both qubits and resonators are coupled to the circuitry environment. The influence of the latter in circuit QED is weak (compared to the order of the bare system frequencies) and, therefore, it suffices to treat it with a master equation of the optical type,

$$\frac{d}{dt}\varrho = -i[H(t),\varrho] + \sum_j \gamma_j\mathcal{D}[\sigma_j]\varrho + \kappa_j\mathcal{D}[a_j]\varrho, \tag{4}$$

where γ_j^{-1} (κ_j^{-1}) accounts for the timescale of relaxation to equilibrium ($\gamma_j^{-1} \sim T_j$) driven by the dissipators, $\mathcal{D}[o_n]\varrho = o_n \varrho o_n^\dagger - \frac{1}{2}(o_n^\dagger o_n \varrho + \varrho o_n^\dagger o_n)$.

III. HAMILTONIAN ENGINEERING

In the following, we will work in the interaction picture with respect to $H_0(t)$, and assume that the qubit gap is modulated as

$$\epsilon_j(t) = \epsilon_j^{(0)} + \sum_{\alpha=\pm} \lambda_{j,\alpha} \cos(\Omega_{j,\alpha} t), \tag{5}$$

for $j = 1, 2$, where $\Omega_{j,\pm}$ represent the driving frequencies given by

$$\Omega_{j,\pm} = \epsilon_j^{(0)} \pm (\omega_j + \delta). \tag{6}$$

In order to validate our approximations, we are going to restrict ourselves to the following hierarchy in parameter space:

$$\epsilon_j^{(0)} \gg \gamma_j \gg \omega_j \gg g_j, J, \delta; \quad \text{and} \quad \Omega_{j,\pm} > \lambda_{j,\pm}. \tag{7}$$

Finally, we assume that $\omega_1 = \omega_2 = \omega$, which is more than plausible due to the well-established and highly reproducible fabrication of superconducting resonators [49]. In our numerical tests, we set $\epsilon_j \cong 5\omega$, $\gamma \cong 2\omega$, and $g \sim J \cong 10^{-2}\omega$. These parameters are reasonable from the experimental point of view and serve to justify all the approximations made below.

The interaction Hamiltonian in the interaction picture with respect to $H_0(t)$ [cf. Eqs. (1)–(3) and (5)] is

$$\begin{aligned}\widetilde{H}_c(t) = {} & J(a_1^\dagger a_2 e^{i(\omega_1-\omega_2)t} + a_1 a_2\, e^{-i(\omega_1+\omega_2)t}) \\ & + g\sigma_1^x(t) a_1 e^{-i\omega_1 t} + g\sigma_2^x(t) a_2 e^{-i\omega_2 t} + \text{H.c.},\end{aligned} \tag{8}$$

where

$$\begin{aligned}\sigma_j^x(t) &= \sigma_j^+ \exp\left[i\epsilon_j^{(0)} t + \sum_\alpha 2i \frac{\lambda_{j,\alpha}}{\Omega_{j,\alpha}} \sin(\Omega_{j,\alpha} t)\right] + \text{H.c.} \\ &= \sigma_j^+ e^{i\epsilon_j^{(0)} t} \prod_\alpha \sum_n J_n\left(\frac{2\lambda_{j,\alpha}}{\Omega_{j,\alpha}}\right) e^{itn\Omega_{j,\alpha}} + \text{H.c.},\end{aligned} \tag{9}$$

with J_n representing the nth Bessel function of the first kind. By choosing $\Omega_{j,\pm}$ according to (6) and recalling the *necessary hierarchy* (7), the Hamiltonian (8) can be approximated (neglecting terms oscillating with $\epsilon_j^{(0)}$) as

$$\begin{aligned}\widetilde{H}_c(t) \cong {} & J(a_1^\dagger a_2 e^{i(\omega_1-\omega_2)t} + a_1 a_2\, e^{-i(\omega_1+\omega_2)t}) \\ & + \sum_j g_j (G_{j+}\sigma_j^+ a_j e^{i\delta t} + G_{j-}\sigma_j^+ a_j^\dagger e^{-i\delta t}) + \text{H.c.},\end{aligned} \tag{10}$$

with $G_{j,\pm}$ given as

$$G_{j,\pm} = J_0\left(2\frac{\lambda_{j,\pm}}{\Omega_{j,\pm}}\right) J_1\left(2\frac{\lambda_{j,\mp}}{\Omega_{j,\mp}}\right). \tag{11}$$

A. Engineering a number-conserving interaction

If the resonator-resonator coupling J is constant, the second term inside the first set of parentheses of (10) can be neglected following the hierarchy (7). Here, we assume that $\omega_1 = \omega_2$.

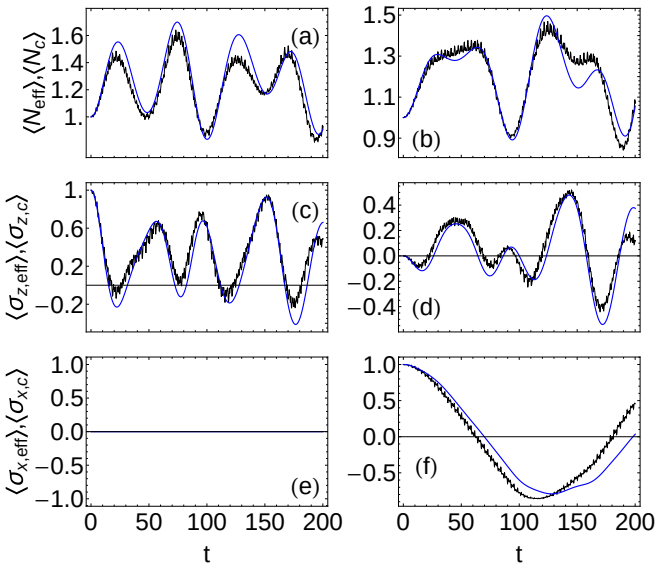

FIG. 2. Time evolution of (a),(b) $\langle N\rangle$, (c),(d) $\langle\sigma_z\rangle$, and (e),(f) $\langle\sigma_x\rangle$ in the proposed circuit-QED architecture according to Eqs. (8) (black) and (12) (blue). For the numerical simulations, we set $\omega = 1$ as the unit. The rest of the parameters used are $\lambda_+ = \lambda_- = 2, \epsilon = 5, \delta = 0.1$, $g = 0.05$, $G_-/G_+ = 0.58$, for (a), (c), (e) the initial state $|\psi(0)\rangle = |\uparrow\rangle|1\rangle$ and (b), (d), (f) the initial state $|\psi(0)\rangle = (|\uparrow\rangle + |\downarrow\rangle)|1\rangle/\sqrt{2}$.

In order to get rid of the extra time dependence (due to δ), we move to a frame rotating with this frequency. Then, the effective Hamiltonian can be written as

$$\begin{aligned}H'_{\rm eff} \cong {} & -\sum_j \delta a_j^\dagger a_j + J(a_1^\dagger a_2 + \text{H.c.}) \\ & + \sum_j g_j[(G_{j+}\sigma_j^+ a_j + G_{j-}\sigma_j^+ a_j^\dagger) + \text{H.c.}].\end{aligned} \tag{12}$$

The validity of the approximations [following the hierarchy (7)] was tested and the results are shown in Figs. 2 and 3 for a single resonator coupled to a qubit. There we show the time evolution under $\widetilde{H}_c(t)$ (8) in black and $H'_{\rm eff}$ (12) in blue. Initial states are $|\phi(t=0)\rangle = |\uparrow\rangle|1\rangle$ (left) and $|\phi(0)\rangle = \frac{1}{\sqrt{2}}[|\uparrow\rangle|1\rangle + |\downarrow\rangle|1\rangle]$ (right). Here, $|\downarrow\rangle$ and $|\uparrow\rangle$ are the ground and excited states of the qubit, respectively, and $|n\rangle$ are the Fock states. We compare the time evolution of *one* resonator of frequency $\omega = 1$ coupled to *one* qubit driven with frequencies Ω_+ and Ω_-, assuming $\delta = 0.1$. The driving amplitudes $\lambda_+ = \lambda_-$ in Fig. 2 are chosen equal, giving a ratio $G_-/G_+ < 1$. In Fig. 3, we choose the $\lambda_\pm$ in such a way that $G_-/G_+ > 1$. It is seen that our approach holds for both the loss- and gain-dominant cases. The fluctuations of the time-dependent Hamiltonian (8) are relatively small and can be made even smaller by decreasing g or increasing ϵ. This is shown on the left-hand side of Figs. 2 and 3, where the values of g and ϵ are smaller and larger, respectively, than their counterparts on the right-hand side.

B. The nonconserving number case

Here we want to exploit the possibility of an on-time tuning of the resonator-resonator coupling [50,51]. By setting

$$J(t) = J\{\cos[(\omega_1 + \omega_2 + 2\delta)t] + \cos[(\omega_1 - \omega_2)t]\}, \tag{13}$$

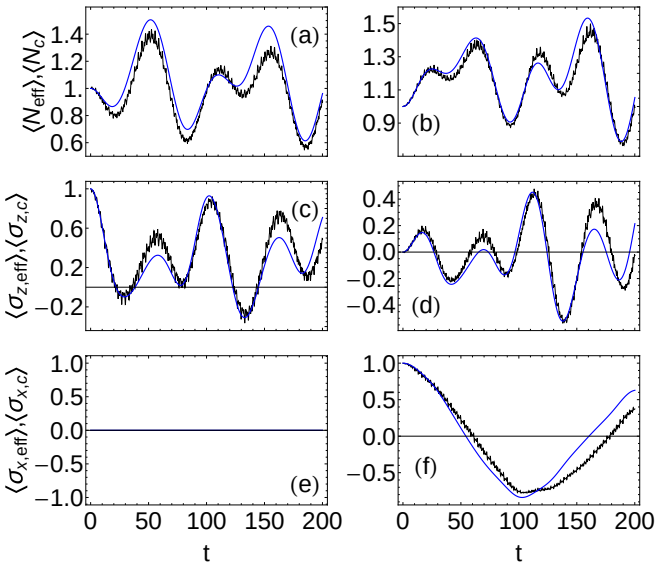

FIG. 3. Time evolution of (a), (b) $\langle N\rangle$, (c), (d) $\langle\sigma_z\rangle$, and (e), (f) $\langle\sigma_x\rangle$ in the proposed circuit-QED architecture according to Eqs. (8) (black) and (10) (blue). For the numerical simulations, we set $\omega = 1$ as the unit. The rest of the parameters used are $\lambda_+ = 3, \lambda_- = 1, \epsilon = 5, \delta = 0.1, g = 0.05, G_-/G_+ = 2.1$, for (a), (c), (e) the initial state $|\psi(0)\rangle = |\uparrow\rangle|1\rangle$ and (b), (d), (f) the initial state $|\psi(0)\rangle = (|\uparrow\rangle + |\downarrow\rangle)|1\rangle/\sqrt{2}$.

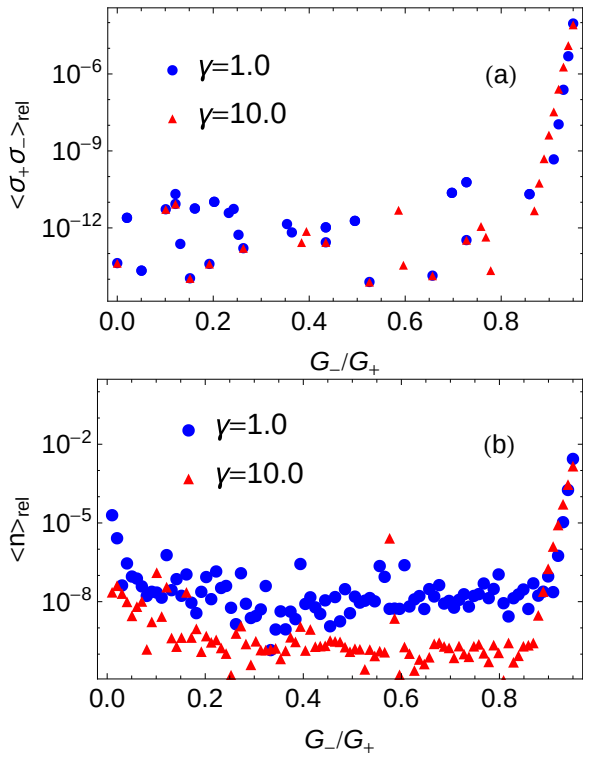

FIG. 4. Numerical verification of the adiabatic elimination for a single resonator coupled to a qubit with decay rates of $\gamma = 1$ and $\gamma = 10$. We use a Fock space of dimension $N_{\text{Fock}} = 300$. In (a), we plot the relative error for $\sigma^+\sigma^-$ as a function of G_-/G_+. In (b), we plot the relative error for $n = a^\dagger a$.

the effective Hamiltonian becomes

$$\begin{aligned} H_{\text{eff}} &\equiv H_{\delta,J} + H_{g_j}^{\text{eff}} \\ &\cong -\sum_j \delta a_j^\dagger a_j + J(a_1^\dagger a_2 + a_1 a_2) \\ &\quad + \sum_j g_j[(G_{j+}\sigma_j^+ a_j + G_{j-}\sigma_j^+ a_j^\dagger) + \text{H.c.}], \end{aligned} \tag{14}$$

where the coupling between resonators includes both the number-preserving terms $a_1^\dagger a_2 + a_1 a_2^\dagger$ and the counter-rotating terms $a_1^\dagger a_2^\dagger + a_1 a_2$. Recall that within the rotating-wave approximation (RWA), the counter-rotating terms are neglected [cf. Eq. (12)]. Therefore, we have an *effective* model which allows us to study physics (beyond the RWA) in the so-called ultra- and deep-strong-coupling regimes (borrowing the nomenclature from the light-matter Rabi model). In our case, it is not the actual coupling strength but the time dependence $J(t)$ or the ratio J/δ which determines whether or not the RWA is valid. The scenario described here serves as a controllable example where RWA versus non-RWA physics may be investigated.

In the following, we will concentrate on the dynamics governed by Eq. (14), but we will compare it with the number-conserving case given in Eq. (12), which is the one mainly studied in the literature.

IV. EFFECTIVE $\mathcal{PT}$ EQUATIONS

A. Adiabatic elimination

Let us now deal with the dissipative part of Eq. (4). The effective timescales in (14) are given by δ, J, and g_j. In the range defined by Eq. (7), the fastest dynamics corresponds to the dissipative evolution of the (bad) qubits: γ_j. In this regime, we can adiabatically eliminate the qubit's degrees of freedom. In doing so, we end up with the slow part, which solely describes an effective dynamics for the two resonators. The technicalities of the adiabatic elimination were already discussed in Ref. [52] and adapted for a similar setup in Ref. [53]. In Appendix A, we give the details of lengthy manipulations, and here we prefer to directly write the effective equations for the first moments of the resonators' operators after eliminating the qubit degrees of freedom,

$$\frac{d}{dt}\langle a_j\rangle = i\langle[H_{\delta,J}, a_j]\rangle + \sum_j \frac{2g_j^2}{\gamma_j}\langle D^\dagger[b_j]a_j\rangle. \tag{15}$$

The b_j operators are defined as [cf. Eq. (11)]

$$b_1 = G_{1,+}\,a_1 + G_{1,-}\,a_1^\dagger, \quad b_2 = G_{2,+}\,a_2 + G_{2,-}\,a_2^\dagger. \tag{16}$$

In order to test the validity of the adiabatic elimination, we compare the *stationary* values obtained from (15) with those obtained from the full quantum master equation given in Eq. (4). In Fig. 4, we plot the relative error between the results obtained from both equations for the stationary values of $\langle\sigma^+\sigma^-\rangle$ and $\langle a^\dagger a\rangle$. We do it for the case of a single resonator coupled to a qubit and as a function of the ratio G_-/G_+. This is the squeezing parameter in the dissipative dynamics of (15) which fully determines the stationary solutions [54]. Our numerical results support the validity of the adiabatic elimination.

B. Verifying the symmetries

To write Eq. (15) in a more convenient way, we define the vector $\vec{\alpha}^t := (\langle a_1\rangle, \langle a_1^\dagger\rangle, \langle a_2\rangle, \langle a_2^\dagger\rangle)$, as well as the effective decay rates

$$\widetilde{\gamma}_j := (-1)^{j+1}\frac{2g_j^2}{\gamma_j}\left(G_{j,-}^2 - G_{j,+}^2\right). \tag{17}$$

Note the $(-1)^{j+1}$ prefactor in the above equation. By setting $G_{1,-} > G_{1,+}$ and $G_{2,-} < G_{2,+}$, we have $\widetilde{\gamma}_j > 0$ always. These relations among the G's imply that resonator 1 is dissipating (i.e., losses are larger than the gain) and resonator 2 is amplifying (i.e., gain is larger than losses). In doing so, Eq. (15) defines the set,

$$i\frac{d}{dt}\vec{\alpha} = M\vec{\alpha}, \tag{18}$$

with

$$M = \begin{pmatrix} \delta - i\widetilde{\gamma}_1 & 0 & J & J \\ 0 & -\delta - i\widetilde{\gamma}_1 & -J & -J \\ J & J & \delta + i\widetilde{\gamma}_2 & 0 \\ -J & -J & 0 & -\delta + i\widetilde{\gamma}_2 \end{pmatrix}. \tag{19}$$

By representing the *unitary* parity operator by

$$\mathcal{P}M\mathcal{P} = (\sigma_x \otimes \mathbb{I}_2)\, M\, (\sigma_x \otimes \mathbb{I}_2), \tag{20}$$

and the *antiunitary* time reversal one by

$$\mathcal{T}M\mathcal{T} = M^*, \tag{21}$$

one can directly verify that in the balanced gain-loss case $\widetilde{\gamma}_1 = \widetilde{\gamma}_2 = \widetilde{\gamma}$, the matrix M is $\mathcal{PT}$ symmetric, i.e., $[\mathcal{PT}, M] = 0$.

V. BROKEN $\mathcal{PT}$-SYMMETRY PHASE

As stated in the introduction, $\mathcal{PT}$-symmetric Hamiltonians may exhibit a real spectrum for certain parameter combinations. The (phase) transition from a complex to a real-valued spectrum occurs at a so-called exceptional point (EP), which marks the degeneracy of a non-Hermitian system, including $\mathcal{PT}$-symmetric systems. At an EP, both the eigenvalues and the corresponding eigenvectors of the Hamiltonian coalesce (i.e., become degenerate). Consequently, the non-Hermitian Hamiltonian governing the system becomes nondiagonalizable. This is significantly different than eigenvalue degeneracies of Hermitian systems where one can always assign orthogonal eigenvectors to degenerate eigenvalues.

In the case of balanced gain and loss, we expect the matrix M to have real eigenvalues in the exact $\mathcal{PT}$-symmetric phase and complex conjugate eigenvalue pairs in the broken $\mathcal{PT}$-symmetric phase. Diagonalizing Eq. (19), we obtain

$$\omega_{\pm\pm} = \pm[\delta^2 - \widetilde{\gamma}^2 \pm 2\delta(J^2 - \widetilde{\gamma}^2)^{1/2}]^{1/2}. \tag{22}$$

By simple inspection, one can immediately see that for $J^2 - \widetilde{\gamma}^2 < 0$, the eigenvalues expressed in Eq. (22) are complex, i.e., the system is in the broken $\mathcal{PT}$ phase. We note that even in this phase, $[\mathcal{PT}, M] = 0$ still holds. The eigenvalues of M are real whenever

$$J > J_{c_1} = \widetilde{\gamma}, \tag{23}$$

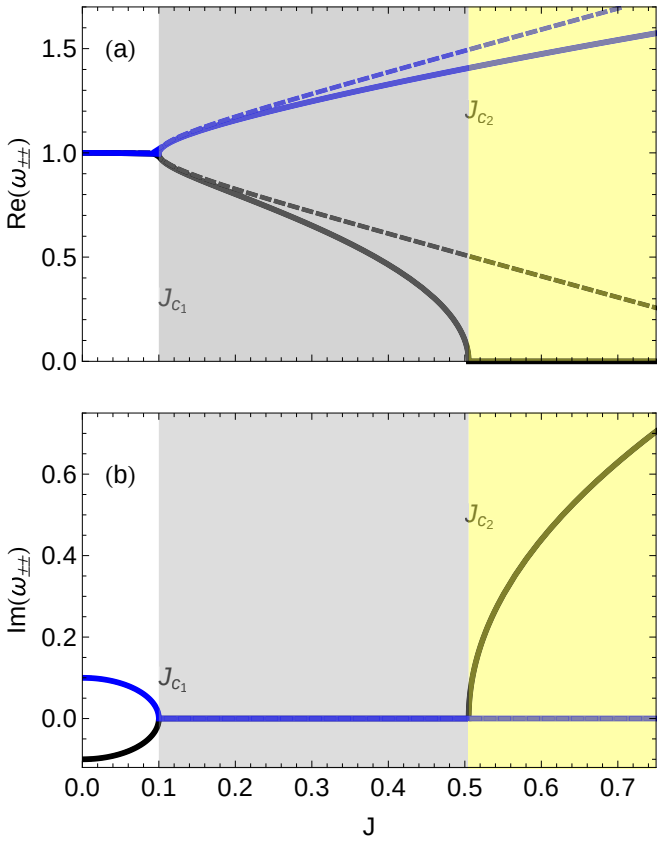

FIG. 5. Evolution of the eigenvalues of the proposed circuit-QED architecture as a function of the resonator-resonator coupling strength J. The background colors distinguish among three regions: $J < J_{c_1}$ (white), $J_{c_1} < J < J_{c_2}$ (light gray), and $J_{c_2} < J$ (light yellow). The eigenfrequency ω_{+-} is plotted in black, while ω_{++} is plotted in blue [cf. Eq. (22)]. The dashed lines correspond to the RWA (12), while the solid lines correspond to the most general case (14). In (a), we plot the real part of $\omega_{+\pm}$ and, in (b), the imaginary part of the eigenvalues. Here we set $\delta = 1$ as the unit and the effective decay rates are $\widetilde{\gamma}_1 = \widetilde{\gamma}_2 = 0.1$.

where J_{c_1} corresponds to the $\mathcal{PT}$-transition point (i.e., *real-to-complex spectral phase transition* point) typically observed in experiments (e.g., in [6,7,55]). Figure 5 shows the evolution of the eigenvalues given in Eq. (22) as a function of the coupling strength J. Here, the dashed lines correspond to the RWA in the resonator-resonator coupling. It is clearly seen that in the RWA model, there is only one transition point located at $J = J_{c_1}$, where the spectra transits from complex to real eigenvalues. In agreement with our discussion of EP's, we notice that at $J = J_{c_1}$, both eigenvalues coincide. In Fig. 5, we can also verify that for the general model given in Eq. (14) (which is beyond the RWA model), there is a second transition at $J = J_{c_2}$ beyond which the eigenvalues become complex again. Thus, in our circuit-QED architecture, real eigenvalues are obtained in the parameter space defined by

$$\widetilde{\gamma} \leqslant J_{c_1} < J < J_{c_2} = \frac{\widetilde{\gamma}^2 + \delta^2}{2\delta}. \tag{24}$$

However, we must be cautious in associating this second transition to a breaking of the $\mathcal{PT}$ symmetry. This is because the

effective Hamiltonian $H_{\delta,J}$ is not positive definite. Therefore, in the absence of dissipation, the eigenfrequencies $\omega_{\pm-}$ are only real for $J < \delta/2$. This bound corresponds to Eq. (24) for $\widetilde{\gamma} = 0$. In the dissipative case, the fact that the eigenvalue ω_{+-} (solid black line in Fig. 5) becomes complex for $J > J_{c_2}$ (blue region) is a reminiscence of the latter. Therefore, this second transition should be understood as an instability point of the driven dissipative system. Another argument to support our claim is that $J = J_{c_2}$ is not an EP.

In Appendix B, we give the general expression for the eigenvalues of the matrix M when the gain and loss are not balanced ($\widetilde{\gamma}_1 \neq \widetilde{\gamma}_2$). In this case, there is *always* a nonzero imaginary contribution to the normal frequencies [cf. Eq. (B1)]. Apart from this offset, the transitions discussed above can also be traced (see Fig. 7).

VI. INPUT-OUTPUT: TRANSMISSION EXPERIMENTS

In the proposed circuit-QED setup, the $\mathcal{PT}$ symmetry can be probed with a simple transmission experiment. Typically, a low-power coherent input $\langle A^{\rm in}\rangle$ is sent into one of the resonators, as depicted in Fig. 1. We label the four ports as $1L$, $1R$, $2L$, and $2R$, where the number indicates resonator 1 or 2 to which the fields are coupled, and the letter R (or L) points out whether the field enters or leaves the circuit from the right (or left) (see Fig. 1). In the figure, the input is sent through $1L$. The transmitted signals (emerging at $1R$,$2L$,$2R$) or the reflected one (emerging at $1L$) can be measured with a vector network analyzer. Indeed, a two-resonator architecture has already been experimentally studied using transmission experiments [41]. Thus, the same techniques can be directly used for the experimental realization of our proposal. Such experiments are described by the input-output theory [56]. The system of interest, in our case the two-resonator two-qubit layout, is coupled to external leads (open transmission lines). We treat both the system and the signals (input and output) quantum mechanically. The fields in the leads are assumed to be bosonic free fields given by

$$H_{\rm leads} = \sum_{j,\lambda} \int d\omega A^{\dagger}_{j,\lambda}(\omega) A_{j,\lambda}(\omega), \tag{25}$$

where $[A_{j,\lambda}(\omega), A_{j',\lambda'}(\omega')^{\dagger}] = \delta_{j,j'}\,\delta_{\lambda,\lambda'}\,\delta(\omega-\omega')$, with $j = 1,2$ and $\lambda = L,R$. Note that the leads act as extra baths for the resonators (adding leakage to the system).

The interaction between the system and the transmission lines (in the case of the proposed setup, a capacitive interaction) is described by the Hamiltonian

$$H_{\rm int} = \sum_{j,\lambda} \int d\omega\, \kappa(\omega)[a_j A^{\dagger}_{j,\lambda}(\omega) + \text{H.c.}]. \tag{26}$$

To obtain the relation for the input and output fields, the Heisenberg equations for the fields $A^{\dagger}_{j,\lambda}$ are considered and Fourier transformed. The input fields, defined as $A^{\rm in}_{j,\lambda}(t) = \int_0^{\infty} d\omega/\sqrt{2\pi}\; A_{j,\lambda}(\omega,t_0)\, e^{-i\omega t}$, take into account contributions from the leads from a time t_0 before the interaction between the input and the system actually occurs. On the other hand, the output fields, defined as $A^{\rm out}_{j,\lambda}(t) = \int_0^{\infty} d\omega/\sqrt{2\pi}\; A_{j,\lambda}(\omega,t_f)\, e^{-i\omega t}$, consider contributions up to a time t_f after the interaction took place. Without loss of generality, a monochromatic signal

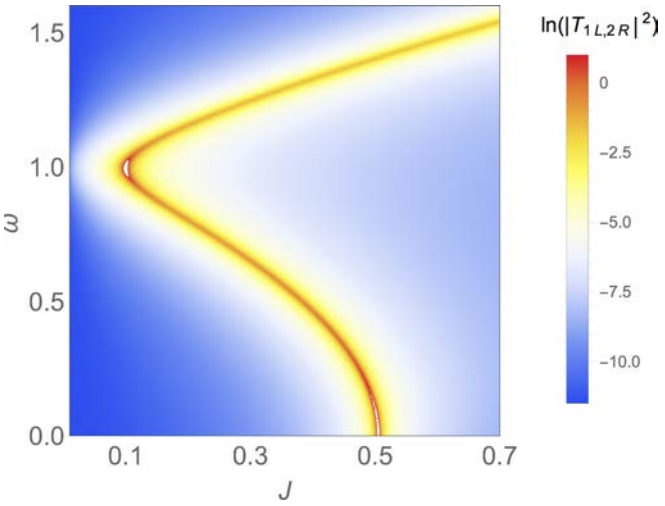

FIG. 6. Logarithm of the power transmitted from port $1L$ to $2R$: $\ln(|T_{1L,2R}|^2)$, as a function of the input frequency ω and resonator-resonator coupling J (in units of frequency). The parameters used in the simulation are $\tilde{\gamma}_1 = \tilde{\gamma}_2 = 0.1$ and $\kappa = 0.02$. The units are the same as those in Fig. 5.

$\langle A^{\rm in}_{1L}\rangle = \alpha e^{i\omega_d t}$ can be used. Following Ref. [56], the input-output relation is

$$\left\langle A^{\rm out}_{j,\lambda}\right\rangle = \left\langle A^{\rm in}_{j,\lambda}\right\rangle - i\sqrt{K}\;\chi_{a_j}^{A^{\rm in}}, \quad j = 1,2; \quad \lambda = L,Rm, \tag{27}$$

where $K = 2\pi\kappa^2(\omega_d)$ is the superconducting resonator leakage through the capacitors, and $\chi_{a_j}^{A^{\rm in}}$ is the linear response of the two-resonator system driven by the input fields. The actual form of $\chi_{a_j}^{A^{\rm in}}$ is rather cumbersome to give here and can be found in Appendix C. Putting all together, the transmitted signal for any of the three ports, $j\lambda = 1R,2R,2L$, is given by

$$T_{1L,j\lambda} = \frac{\left\langle A^{\rm out}_{j,\lambda}\right\rangle}{\left\langle A^{\rm in}_{1L}\right\rangle}. \tag{28}$$

The transmission with an input through any of the other ports can be calculated in the same way.

In Fig. 6, we depict $T_{1L,2R}$ as a function of the coupling and the input frequency. As expected, the contour plot resembles the real frequency plot in Fig. 5(a). The maximum in the transmission coincides with the resonance frequencies. Therefore, in a transmission experiment, the $\mathcal{PT}$ symmetry can be directly tested.

VII. CONCLUSIONS

In this work, we have shown that a circuit-QED architecture provides a flexible and highly versatile platform, with a small footprint, to explore the physics of non-Hermitian $\mathcal{PT}$ systems. Understanding that the latter is an effective theory, we have demonstrated how $\mathcal{PT}$ symmetry and its breaking emerges by engineering two-resonator two-qubit Hamiltonian systems using tunable external drives, which is a natural strategy in circuit-QED systems.

This architecture has allowed us to probe the resonator-resonator interactions in various regimes of interaction strength thanks to the ability to achieve tunable coupling strength in circuit QED, provided tunable gain and loss to delicately

control the gain-loss ratio of the resonators, and opened the way to probe non-Hermitian dynamics in coupling regimes, ranging from weak to deep coupling not only in the interaction between the resonators but in the interaction between the resonators and the qubits coupled to them for achieving gain and loss. We have shown that in the weak-coupling regime of the resonator-resonator interaction, the $\mathcal{PT}$ symmetry is broken, i.e., the effective Hamiltonian exhibits nonreal eigenvalues.

By increasing the coupling, non-number-conserving terms start to play a significant role. This is the *ultrastrong*-coupling regime that has already been explored experimentally in superconducting circuits [41,57]. In the $\mathcal{PT}$ scenario, this region corresponds to the unbroken (or the exact) $\mathcal{PT}$-symmetric phase. At much higher coupling strengths, the resonators become unstable. Crucially, this last transition is absent if we neglect the counter-rotating terms. This regime corresponds to the *deep-strong*-coupling regime. More importantly, weak, strong, ultrastrong, and deep-strong regimes are differentiated by transition points (either breaking symmetry or instability). We note that in previous studies (Rabi model [58–61]) where the qubit-resonator coupling was investigated in various coupling regimes, the borders between different regimes were diffuse. Revisiting those studies by considering the $\mathcal{PT}$-symmetric resonator-resonator configuration proposed here may shed light on how different regimes in resonator-resonator coupling affect the quantum dynamics.

Finally, we have shown that the proposed circuit-QED architecture is experimentally accessible; no fine tuning of the experimental parameters is necessary in order to observe the phenomenology imposed by $\mathcal{PT}$ symmetry, and the basic concepts and applications that have been demonstrated in other platforms can be accessed and realized in this circuit-QED platform with a simple transmission experiment. We thus believe that this work will open the way to use circuit QED as an ideal testbed to explore $\mathcal{PT}$-symmetric physics in the quantum domain.

ACKNOWLEDGMENTS

We would like to thank Göran Johansson for valuable discussions. F.Q. acknowledges financial support from the Swedish Research Council and the Knut and Alice Wallenberg Foundation. S.K.O. is supported by ARO Grant No. W911NF-18-1-0043 and by The Pennsylvania State University, Materials Research Institute. F.N. is partially supported by the MURI Center for Dynamic Magneto-Optics via the AFOSR Award No. FA9550-14-1-0040, the Japan Society for the Promotion of Science (KAKENHI), the IMPACT program of JST, CREST Grant No. JPMJCR1676, RIKEN-AIST Challenge Research Fund, JSPS-RFBR Grant No. 17-52-50023, and the Sir John Templeton Foundation. D.Z. acknowledges support by the Spanish Ministerio de Economia y Competitividad within Projects No. MAT2014- 53432-C5-1-R and No. FIS2014-55867 and the Gobierno de Aragon (FENOL group). F.Q., S.K.O., and D.Z. acknowledge the hospitality of Riken where part of this work was done.

APPENDIX A: ADIABATIC ELIMINATION

Here we provide the details of the *adiabatic elimination*. We consider a system (resonator) coupled to the environment through an ancillary element (qubit). The adiabatic elimination is rooted in the fact that the relaxation timescale of the ancilla is much faster than the typical timescale in which the system evolves [cf. the hierarchy given by Eq. (7)].

1. Single-resonator case

For the case of a single resonator, after driving the qubit and neglecting the rotating terms, we are left with the following Hamiltonian (in the interaction picture):

$$\widetilde{H}_c = g(b\sigma^+ + b^\dagger\sigma^-), \quad b := G_- a + G_+ a^\dagger \tag{A1}$$

[cf. Eq. (12); for a single resonator $J = 0$ and we consider $\delta = 0$]. Coupling the qubit to an environment and assuming Markovianity leads to the following nonunitary evolution for the combined system of the resonator and the qubit (this is valid provided that $\epsilon \gg \gamma \gg g$):

$$d_t\varrho = L_0[\varrho] + L_1[\varrho], \tag{A2}$$

where the state ϱ lives in the total Hilbert space ($\mathcal{H}$) of the resonator ($\mathcal{H}_{\rm res}$) and the qubit ($\mathcal{H}_{\rm qub}$): $\mathcal{H} = \mathcal{H}_{\rm res} \otimes \mathcal{H}_{\rm qub}$. In addition, we have defined the Liouvillian operators,

$$L_0[\varrho] = \frac{\gamma}{2}(2\sigma^-\varrho\sigma^+ - \{\sigma^+\sigma^-,\varrho\}) \tag{A3}$$

and

$$L_1[\varrho] = -i[\widetilde{H}_c,\varrho]. \tag{A4}$$

We will treat the L_1 part of the Liouvillian as a perturbation over L_0 (recall that $\gamma \gg g$). For this, we define the operator

$$\bar{\varrho} = \exp(-L_0 t)\varrho, \tag{A5}$$

which evolves in time according to

$$d_t\bar{\varrho} = \bar{L}_1\bar{\varrho}, \tag{A6}$$

with

$$\bar{L}_1 = e^{-L_0 t} L_1 e^{L_0 t}. \tag{A7}$$

In order to deal with (A6), we will make use of projection operator techniques. The idea behind this method is to introduce two orthogonal projections, represented by the superoperators $\mathcal{R}$ and $\mathcal{Q}$, with $\mathcal{R}^2 = \mathcal{R}$, $\mathcal{Q}^2 = \mathcal{Q}$, $\mathcal{RQ} = \mathcal{QR} = 0$, and $\mathcal{R} + \mathcal{Q} = \mathbb{I}$. This allows us to split the total density matrix ϱ in a relevant part μ describing the resonator and in an irrelevant part describing the qubit $\varrho_{\rm qub}$. The action of $\mathcal{R}$ and $\mathcal{Q}$ on $\bar{\varrho}$ is defined by

$$\mathcal{R}\bar{\varrho} = {\rm tr}_{\rm qub}(\bar{\varrho}) \otimes \varrho_{\rm qub} = \mu \otimes \varrho_{\rm qub}, \tag{A8}$$

$$\mathcal{Q}\bar{\varrho} = (\mathbb{I} - \mathcal{R})\bar{\varrho}. \tag{A9}$$

Here, $\varrho_{\rm qub}$ denotes some fixed state of the qubit. If we assume that the qubit undergoes a strongly dissipative dynamics, and in the absence of a pump, we can safely assume this state to be the ground state, $\varrho_{\rm qub} = |\downarrow\rangle\langle\downarrow|$. As L_0 acts on the space of the qubit and $\mathcal{R}$ projects on the orthogonal space, these two superoperators commute, $[L_0,\mathcal{R}] = 0$. This guarantees that $\mathcal{R}\bar{\varrho} = \mathcal{R}\varrho$. Applying $\mathcal{R}$ and $\mathcal{Q}$ to (A6), we arrive at the

following system:

$$d_t \mathcal{R}\bar{\varrho} = \mathcal{R}\bar{L}_1\mathcal{R}\bar{\varrho} + \mathcal{R}\bar{L}_1\mathcal{Q}\bar{\varrho}, \tag{A10}$$

$$d_t \mathcal{Q}\bar{\varrho} = \mathcal{Q}\bar{L}_1\mathcal{Q}\bar{\varrho} + \mathcal{Q}\bar{L}_1\mathcal{R}\bar{\varrho}. \tag{A11}$$

We first solve (A11),

$$\mathcal{Q}\bar{\varrho}(t) = \mathcal{G}(t,0)\mathcal{Q}\bar{\varrho}(0) + \int_0^t ds\, \mathcal{G}(t,s)\mathcal{Q}\bar{L}_1(s)\mathcal{R}\bar{\varrho}(s), \tag{A12}$$

where $\mathcal{G}$ denotes the time-ordered exponential,

$$\mathcal{G}(t,s) = \mathcal{T}\exp\left[\int_s^t ds'\mathcal{Q}\bar{L}_1(s')\right], \tag{A13}$$

which is the formal solution of

$$d_t \mathcal{Q}\bar{\varrho} = \mathcal{Q}\bar{L}_1\mathcal{Q}\bar{\varrho}, \tag{A14}$$

where $\bar{L}_1$ is time dependent. We now substitute (A12) into (A10) to obtain the so-called Nakajima-Zwanzig equation,

$$d_t \mathcal{R}\bar{\varrho} = \mathcal{R}\bar{L}_1\mathcal{R}\bar{\varrho} + \mathcal{R}\bar{L}_1\mathcal{G}(t,0)\mathcal{Q}\bar{\varrho}(0) + \mathcal{R}\bar{L}_1\int_0^t ds\, \mathcal{G}(t,s)\mathcal{Q}\bar{L}_1(s)\mathcal{R}\bar{\varrho}(s). \tag{A15}$$

We can further simplify this equation as follows: from (A5), it follows that $\bar{\varrho}(0) = \varrho(0)$. If we assume an initial factorized state, the action of $\mathcal{R}$ on it is equal to the action of the identity operator, and therefore $\mathcal{Q}\bar{\varrho}(0) = 0$. We now turn back to the equation for the state ϱ. From (A5), it follows

$$\mathcal{R}\mathrm{e}^{-L_0 t}d_t\varrho = d_t\mathcal{R}\bar{\varrho} + L_0\mathcal{R}\bar{\varrho}. \tag{A16}$$

Replacing (A15) in the former equation leads to

$$\mathcal{R}e^{-L_0 t}d_t\varrho = \mathcal{R}\bar{L}_1\mathcal{R}\bar{\varrho} + \mathcal{R}\bar{L}_1\int_0^t ds\, \mathcal{G}(t,s)\mathcal{Q}\bar{L}_1(s)\mathcal{R} + \mathcal{R}L_0\mathcal{R}\bar{\varrho}(s), \tag{A17}$$

where we have made use of the fact that $\mathcal{R}\mathcal{Q}\varrho = \mathcal{R}\varrho - \mathcal{R}^2\varrho = 0$. As usual, we will assume $\mathcal{R}L\mathcal{R} = 0$ [62] for the full Liouvillian $L = L_0 + L_1$. In our case, this implies

$$\mathcal{R}\bar{L}_1\mathcal{R}\bar{\varrho} + \mathcal{R}L_0\mathcal{R}\bar{\varrho} = 0. \tag{A18}$$

Thus, we are left with

$$\mathcal{R}e^{-L_0 t}d_t\varrho = \mathcal{R}\bar{L}_1\int_0^t ds\, \mathcal{G}(t,s)\mathcal{Q}\bar{L}_1(s)\mathcal{R}. \tag{A19}$$

The lowest-order expansion in the perturbation L_1 involves taking $\mathcal{G}(t,s) = \mathbb{I}$. This corresponds to second-order perturbation theory as L_1 already appears twice in the right-hand side. Thus, from (A7), we finally have

$$d_t\mathcal{R}\varrho = \mathcal{R}L_1\int_0^t ds\exp[L_0(t-s)]L_1\mathcal{R}\varrho(s). \tag{A20}$$

Tracing over the qubit, we arrive at a quantum master equation (QME) describing the effective dissipative dynamics of the resonator,

$$d_t\mu = -\int_0^t ds\,\mathrm{tr}_{\mathrm{qub}}\{\widetilde{H}_c\,, \exp[L_0(t-s)][\widetilde{H}_c\,,\mu(s)\otimes\varrho_{\mathrm{qub}}]\}. \tag{A21}$$

We perform the following change of variables $s' = t - s$ and apply the Markov approximation, that is, $\mu(t-s') \to \mu(t)$. The final step consists of tracing out the qubit degrees of freedom. For this, we notice that $\sigma^{\pm}$ are eigenoperators of L_0 with eigenvalue $-\gamma/2$ [$L_0\sigma^{\pm} = -(\gamma/2)\sigma^{\pm}$]. Then, it is straightforward to show

$$\begin{aligned}[\widetilde{H}_c\,, e^{L_0 s}(\widetilde{H}_c\,,\mu\otimes\varrho_{\mathrm{qub}})] &= \exp[-(\gamma/2)s]g^2([b^\dagger, b\mu] - [b, \mu b^\dagger]) \\ &= \exp[-(\gamma/2)s]g^2(-2b\mu b^\dagger + \{b^\dagger b, \mu\}).\end{aligned} \tag{A22}$$

Then, Eq. (A21) reduces to

$$d_t\mu = \int_0^t ds\exp[-(\gamma/2)s]g^2(2b\mu b^\dagger - \{b^\dagger b,\mu\}). \tag{A23}$$

Finally, integrating over time, in the limit $t\to\infty$ we obtain our desired result,

$$d_t\mu = \frac{2g^2}{\gamma}(2b\mu b^\dagger - \{b^\dagger b,\mu\}). \tag{A24}$$

The role of the b operators is clear now. Using the drive on the auxiliary qubits, the effective dissipative dynamics on the resonator can have a nontrivial (not Gibbs) long-time dynamics. For example, whenever $G_-^2 - G_+^2 = 1$, the b operators become *squeezed vacuum annihilator operators* and, therefore, the stationary solution of Eq. (A24) is a squeezed vacuum state.

2. Coupled resonators

Here we generalize the results derived for the single-resonator case to a chain of coupled cavities. We consider one-dimensional, regular, and nearest-neighbor coupling between resonators in an array. We consider two types of coupling. The first is what we call the RWA coupling, $\sim a_j^\dagger a_{j+1} + \mathrm{H.c.}$ This conserves the total number of excitations in the lattice.

The second type is called the non-RWA coupling, which does not conserve the number of excitations, $\sim(a_j + a_j^\dagger)(a_{j+1} + a_{j+1}^\dagger)$. This appears naturally in dipole-dipole or displacement couplings in electromagnetic or mechanical systems.

Usually, the RWA coupling corresponds to the non-RWA in the weak-coupling regime. We emphasize that here both types of couplings are engineered. Therefore, it is not the interaction strength [always small; see (7)] but the driving fields (cf. Secs. III and III B) which dictate the type of coupling.

a. RWA coupling

We start by manipulating the coherent part of H in Eq. (1),

$$H = H_0 + H_c + H_{\mathrm{drive}}, \tag{A25}$$

with

$$H_0 = \sum_j\left(\frac{\epsilon}{2}\sigma_j^z + \omega a_j^\dagger a_j\right), \tag{A26}$$

$$H_c = \sum_j g\sigma_j^x(a_j^\dagger + a_j) + J(a_j^\dagger + a_j)(a_{j+1}^\dagger + a_{j+1}), \tag{A27}$$

$$H_{\mathrm{drive}} = \sum_j\sum_\alpha \lambda_\alpha\cos(\Omega_\alpha t)\sigma_j^z, \tag{A28}$$

where, for simplicity, we assume that all resonators have the same frequency ω_r and all qubits have the same transition frequency ϵ. Also, we assume that every resonator is coupled to its own qubit with the same strength g and that the driving amplitudes are site independent. Expanding the resonator operators in momentum space (plane-wave basis), $a_k = N^{-1/2}\sum_j e^{-ikj}a_j$, with $k \in 2\pi/N \times \mathbb{Z}$, we can rewrite the total Hamiltonian as

$$H = H_0' + H_c' + H_{\text{drive}}, \tag{A29}$$

where

$$H_0' = \sum_j \frac{\epsilon}{2}\sigma_j^z + \sum_k \varepsilon_k a_k^\dagger a_k, \tag{A30}$$

$$H_c' = \sum_{k,j} g(e^{-ijk}\sigma_j^x a_k^\dagger + \text{H.c.}), \tag{A31}$$

with $\varepsilon_k = \omega + 2J\cos(k)$. The latter is valid whenever $\omega_r \gg J$. In this limit, the plane-wave basis diagonalizes the intercavity interaction. In the interaction picture with respect to $H_0' + H_{\text{drive}}$, the interaction Hamiltonian is written as

$$\widetilde{H}_c'(t) = \sum_{k,j} g\{e^{ijk}(\sigma_j^+ e^{2if(t)} + \sigma_j^- e^{-2if(t)})a_k e^{-i\varepsilon_k t} + \text{H.c.}\}, \tag{A32}$$

where the time-dependent term is given by

$$f(t) = \frac{\epsilon}{2}t + \sum_\alpha \frac{\lambda_\alpha}{\Omega_\alpha}\sin(\Omega_\alpha t), \tag{A33}$$

as can easily be obtained by integration. Now, we make use of the Jacobi-Anger expansion for the exponential terms,

$$\exp[2if(t)] = \exp\left\{i\left[\epsilon t + 2\sum_\alpha \frac{\lambda_\alpha}{\Omega_\alpha}\sin(\Omega_\alpha t)\right]\right\} \tag{A34}$$

$$= \exp(i\epsilon t)\prod_\alpha \exp\left[2i\frac{\lambda_\alpha}{\Omega_\alpha}\sin(\Omega_\alpha t)\right] \tag{A35}$$

$$= \exp(i\epsilon t)\prod_\alpha \sum_{n=-\infty}^{+\infty} J_n\left(2\frac{\lambda_\alpha}{\Omega_\lambda}\right)\exp[in(\Omega_\alpha t)], \tag{A36}$$

where J_n is the nth Bessel function of the first kind. Up to first order in the ratio $\lambda_\alpha/\Omega_\alpha \to 0$, we can safely neglect all orders of J_n, except $n = \pm 1, 0$. In addition, we select two driving frequencies ($\alpha = -, +$) $\Omega_- = \epsilon - (\omega + \delta)$ and $\Omega_+ = \epsilon + (\omega + \delta)$. According to our established hierarchy, $\epsilon \gg \omega$, we can neglect all the fast rotating terms. Therefore, we are left with

$$\exp[2if(t)] = J_0\left(2\frac{\lambda_-}{\Omega_-}\right)J_1\left(2\frac{\lambda_+}{\Omega_+}\right)\exp[-i(\omega_r + \delta)t] + J_0\left(2\frac{\lambda_+}{\Omega_+}\right)J_1\left(2\frac{\lambda_-}{\Omega_-}\right)\exp[i(\omega_r + \delta)t]. \tag{A37}$$

In order to simplify the notation, we will define

$$G_+ = J_0\left(2\frac{\lambda_+}{\Omega_+}\right)J_1\left(2\frac{\lambda_-}{\Omega_-}\right), \tag{A38}$$

$$G_- = J_0\left(2\frac{\lambda_-}{\Omega_-}\right)J_1\left(2\frac{\lambda_+}{\Omega_+}\right). \tag{A39}$$

Thus,

$$\exp[2if(t)] = G_-\exp[-i(\omega + \delta)t] + G_+\exp[i(\omega + \delta)t]. \tag{A40}$$

Substituting (A40) in (A32) yields

$$\widetilde{H}_c'(t) = \sum_{kj} g(G_+ e^{ikj}\exp[i(\omega - \epsilon_k + \delta)t]a_k + G_- e^{-ikj}\exp[-i(\omega - \epsilon_k + \delta)t]a_k^\dagger)\sigma_j^+ + \text{H.c.}$$
$$= \sum_{kj} g(G_+ e^{ikj}\exp\{-i[2J\cos(k) - \delta]t\}a_k + G_- e^{-ikj}\exp\{i[2J\cos(k) - \delta]t\}a_k^\dagger)\sigma_j^+ + \text{H.c.} \tag{A41}$$

or

$$\widetilde{H}_c'(t) = \sum_j g(b_j(t)\sigma_j^+ + \text{H.c.}), \tag{A42}$$

with $b_j(t)$ given by

$$b_j(t) = \sum_k (G_+ e^{ikj}\exp\{-i[2J\cos(k) - \delta]t\}a_k + G_- e^{-ikj}\exp\{i[2J\cos(k) - \delta]t\}a_k^\dagger). \tag{A43}$$

We will now proceed with the master equation,

$$\frac{d\varrho}{dt} = L_0(\varrho) + L_1(\varrho). \tag{A44}$$

Here, L_0 describes the dissipation induced by the bath on the qubits (recall that we only take into account spontaneous-emission processes), and therefore

$$L_0(\varrho) = \sum_j \frac{\gamma}{2}(2\sigma_j^-\varrho\sigma_j^+ - \sigma_j^+\sigma_j^-\varrho - \varrho\sigma_j^+\sigma_j^-), \tag{A45}$$

while L_1 describes the unitary evolution due to the coupling: $L_1\varrho = -i[\widetilde{H}_c'(t), \varrho]$.

We want to study the dissipative dynamics induced on the resonators by the qubits. For a strong dissipative dynamics of the qubits, it is safe to assume that they remain fixed in the ground state. Therefore, we can adiabatically eliminate the degrees of freedom of the qubits. We start by defining the

projector P,

$$P\varrho = \mu \otimes \varrho_{q,ss} = \mu \otimes \varrho_{q1,ss} \otimes \cdots \otimes \varrho_{qi,ss} \cdots \otimes \varrho_{qN,ss}. \tag{A46}$$

Here, μ describes the system of resonators and we take the ground state of all the qubits $\varrho_{qi,ss} = |\downarrow\rangle_{ii}\langle\downarrow|$ as a fixed state. In second-order perturbation theory (in L_1), we obtain the following effective dynamics for the resonators:

$$\frac{d\mu}{dt} = -\int_0^\infty d\tau\, \mathrm{Tr}_\mathrm{q}\{\widetilde{H}_c'(t), e^{L_0\tau}[\widetilde{H}_c'(t-\tau), \mu(t)\otimes\varrho_{q,ss}]\}, \tag{A47}$$

where the Born-Markov approximation has already been performed. Expanding the commutators in (A47), we can perform the partial trace over the qubits. For this, we must take into account (A42) and that σ_j^+ and σ_j^- are eigenstates of the superoperator L_0, both with eigenvalue $-\gamma/2$. Thus, we are left with

$$\frac{d\mu}{dt} = \int_0^\infty d\tau\, e^{-\gamma/2\tau} \sum_j g^2\{[b_j^\dagger(t), b_j(t-\tau)\mu(t)] - [b_j(t), \mu(t)b_j^\dagger(t-\tau)]\}. \tag{A48}$$

Expanding the $b_j(t)$ operators and performing the integration over the variable τ yields

$$\int_0^\infty d\tau\, \exp(-\{\gamma/2 \pm i[2J\cos(k)+\delta]\}\tau) = \frac{2/\gamma}{1 \pm 2i[2J\cos(k)+\delta]/\gamma} = \frac{2}{\gamma}, \tag{A49}$$

which follows from the hierarchy of energies considered in this work [cf. Eq. (7)]. From this, we arrive at the QME in the interaction picture in position space,

$$\frac{d\mu}{dt} = \frac{2g^2}{\gamma}\sum_j 2b_j(t)\mu(t)b_j^\dagger(t) - \{b_j^\dagger(t)b_j(t), \mu(t)\}. \tag{A50}$$

We note that $\gamma \gg J$ is required to arrive at (A50). In fact, the time evolution of the b_j operators could be more intricate, i.e., nonreducible to an analytic expression. For a general evolution operator U, the time evolution is given by $b_j(t) = U^\dagger(t)b_j(0)U(t)$. Assuming a time-independent Hamiltonian H, we have $U(t) = \exp(-iHt)$. Decomposing the latter into eigenstates of H ($H|\alpha\rangle = E_\alpha|\alpha\rangle$) leads to $U(t) = \sum_\alpha \exp(-iE_\alpha t)|\alpha\rangle\langle\alpha|$. Performing the time integration in (A48) will lead to terms of the form

$$\int_0^\infty d\tau\, e^{-\gamma/2\tau} b_j(t-\tau) = \sum_{\alpha\beta} e^{i(E_\beta - E_\alpha)t}\int_0^\infty d\tau\, e^{-[\gamma/2 - i(E_\alpha - E_\beta)]\tau}|\beta\rangle\langle\beta|b_j(0)|\alpha\rangle\langle\alpha|. \tag{A51}$$

If the characteristic energies associated to H are much smaller than the coupling to the environment ($\gamma \gg E_\alpha$), we again have, for the integral,

$$\int_0^\infty d\tau\, \exp\{-[\gamma/2 - i(E_\alpha - E_\beta)]\tau\} = \frac{2/\gamma}{1 - 2i(E_\alpha - E_\beta)/\gamma} = \frac{2}{\gamma}. \tag{A52}$$

Therefore,

$$\int_0^\infty d\tau\, \exp(-\gamma/2\tau) b_j(t-\tau) = \frac{2}{\gamma}\sum_{\alpha\beta} e^{i(E_\beta - E_\alpha)t}|\beta\rangle\langle\beta|b_j(0)|\alpha\rangle\langle\alpha| = \frac{2}{\gamma}b_j(t), \tag{A53}$$

and similarly for the Hermitian conjugated terms. This leads again to Eq. (A50).

The final step consists of going back to the Schrödinger picture and expressing the QME in momentum space. From (A43), the momentum-space operators a_k evolve in time according to $a_k \exp\{-i[2J\cos(k) - \delta]t\}$. Going back to the Schrödinger picture implies canceling out these rotating terms. We can fulfill this condition by applying the following transformation:

$$a_k = U_0(t)a_k(t)U_0^\dagger(t), \tag{A54}$$

with $U_0(t) = \exp\{-i[2J\cos(k) - \delta]t\}$, to both sides of (A50). Doing so, we arrive to the desired result,

$$\frac{d\mu}{dt} = \sum_k -i\omega_k[a_k^\dagger a_k, \mu] + \frac{2g^2}{\gamma}(2b_k\varrho b_k^\dagger - \{b_k^\dagger b_k, \mu\}), \tag{A55}$$

where we have defined $\omega_k = 2J\cos(k) - \delta$, and $b_k = G_+a_k + G_-a_{-k}^\dagger$.

b. Non-RWA coupling

Following Sec. III B, after engineering H by means of a two-color driving and a time-dependent coupling $J(t)$, we arrive at the effective Hamiltonian,

$$H_\mathrm{eff}^\mathrm{nRWA} = -\sum_j \delta a_j^\dagger a_j + J(a_j^\dagger + a_j)(a_{j+1}^\dagger + a_{j+1}) + \sum_j g(G_{j+}\sigma_j^+ a_j + G_{j-}\sigma_j^+ a_j^\dagger + \mathrm{H.c.}). \tag{A56}$$

In order to obtain the dissipative dynamics for the resonators, we proceed as we did in the previous section. However, instead of moving to the momentum space, we rewrite $H_\mathrm{eff}^\mathrm{nRWA}$ in an interaction picture with respect to $\bar{H} = -\sum_j \delta a_j^\dagger a_j + J(a_j^\dagger + a_j)(a_{j+1}^\dagger + a_{j+1})$. This leads to

$$H_\mathrm{eff}^\mathrm{nRWA}(t) = \sum_j g[G_{j+}a_j(t)\sigma_j^+ + G_{j-}a_j^\dagger(t)\sigma_j^+ + \mathrm{H.c.}], \tag{A57}$$

where $a_j(t) = e^{i\bar{H}t} a_j e^{-i\bar{H}t}$. By introducing the operators $b_j(t) = G_{j+}a_j(t) + G_{j-}a_j^\dagger(t)$, the above yields

$$H_{\rm eff}^{\rm nRWA}(t) = \sum_j g[b_j(t)\sigma_j^+ + {\rm H.c.}]. \tag{A58}$$

Here, we do not know the explicit time dependence of the b_j operators. Assuming again a strong dissipation for the qubits, we can follow the general steps in Eqs. (A44)–(A48). Regardless of the explicit evolution of the b_j's, whenever the energy scale associated with the transformation Hamiltonian (in this case $\bar{H}$) is much smaller than γ [as dictated by Eq. (7)], we can always reduce (A48) to (A50). Going back to the Schrödinger picture, we obtain

$$\frac{d\mu}{dt} = -i\left[\sum_j -\delta a_j^\dagger a_j + J(a_1^\dagger + a_1)(a_2^\dagger + a_2), \mu\right] + \frac{2g^2}{\gamma}\sum_j 2b_j\mu b_j^\dagger - \{b_j^\dagger b_j, \mu\}. \tag{A59}$$

APPENDIX B: EIGENVALUES FOR THE CASE OF UNBALANCED GAIN AND LOSS

Diagonalizing Eq. (18) for the general (i.e., unbalanced gain and loss) case $\tilde{\gamma}_1 \neq \tilde{\gamma}_2$, we obtain the eigenfrequencies

$$\omega'_{\pm\pm} = \pm\left\{\delta^2 - \frac{(\tilde{\gamma}_1+\tilde{\gamma}_2)^2}{4} \pm 2\delta\left[J^2 - \frac{(\tilde{\gamma}_1+\tilde{\gamma}_2)^2}{4}\right]^{1/2}\right\}^{1/2} + i\frac{\tilde{\gamma}_2-\tilde{\gamma}_1}{2}. \tag{B1}$$

It is seen that whenever $\tilde{\gamma}_1 \neq \tilde{\gamma}_2$, there is no region in the parameter space where (B1) is real (i.e., no complex part). However, the eigenvalues may or may not coincide in their real or imaginary parts, depending on the square roots in (B1). The generalizations of the critical values (23) and (24) to the imbalanced case therefore are

$$J < J'_{c1} = \frac{\tilde{\gamma}_1+\tilde{\gamma}_2}{2} \tag{B2}$$

and

$$J'_{c2} = \frac{(\tilde{\gamma}_1+\tilde{\gamma}_2)^2 + 4\delta^2}{8\delta} < J. \tag{B3}$$

This general behavior, for both RWA and non-RWA cases, is shown in Fig. 7. There is always a nonzero imaginary contribution to the normal frequencies [cf. last term in (B1)]. Even in this case, the phase transitions are clearly seen.

APPENDIX C: INPUT-OUTPUT

In a fully quantum treatment, the system (in our case, the two-resonator two-qubit circuit) and the input-output transmission lines (cf. Fig. 1) are formally described by the Hamiltonian

$$H = H_{\rm sys} + \sum_{j,\lambda}\int d\omega A_{j,\lambda}^\dagger(\omega)A_{j,\lambda}(\omega) + \sum_j \kappa_{j,\lambda}(\omega)[a_j A_{j,\lambda}^\dagger(\omega) + {\rm H.c.}], \tag{C1}$$

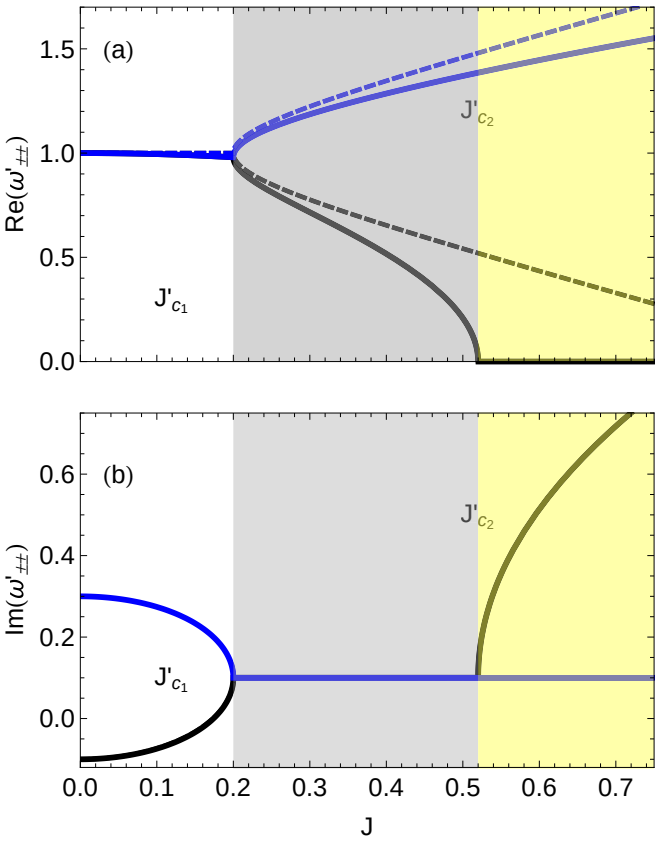

FIG. 7. Eigenfrequencies for the case of unbalanced gain and loss between the resonators (B1) as a function of the resonator-resonator coupling strength J. The background colors distinguish among three regions: $J < J'_{c_1}$ (white), $J'_{c_1} < J < J'_{c_2}$ (light gray), and $J'_{c_2} < J$ (light yellow) [cf. Eqs. (B2) and (B3)]. The eigenfrequency ω'_{+-} is plotted in black, while ω'_{++} is plotted in blue. The dashed lines correspond to the RWA (12), while the solid lines correspond to the most general case (14). In (a), we plot the real part of $\omega'_{+\pm}$ and, in (b), the imaginary part. Here we set $\delta = 1$ as the unit and the effective decay rates are $\tilde{\gamma}_1 = 0.1$, $\tilde{\gamma}_2 = 0.3$.

with $[A_{j,\lambda}(\omega), A_{j',\lambda'}(\omega')^\dagger] = \delta_{j,j'}\,\delta_{\lambda,\lambda'}\,\delta(\omega-\omega')$ the quantized modes in the input lines. Here we use the same labeling $j = 1,2$, and $\lambda = L, R$, for different ports, as described in the main text. For the sake of simplicity, we will consider that both resonators are equally and symmetrically coupled to the corresponding transmission lines.

The Heisenberg equations for the operators $A_{j,\lambda}(\omega)$, together with the definitions,

$$A_{j,\lambda}^{\rm in}(t) = \int_0^\infty d\omega/\sqrt{2\pi}\; A_{j,\lambda}(\omega,t_0)\,e^{-i\omega t}, \tag{C2}$$

$$A_{j,\lambda}^{\rm out}(t) = \int_0^\infty d\omega/\sqrt{2\pi}\; A_{j,\lambda}(\omega,t_f)\,e^{-i\omega t}, \tag{C3}$$

yield the following relation for the output and input fields:

$$A_{j,\lambda}^{\rm out}(t) = A_{j,\lambda}^{\rm in}(t) - i\int_0^\infty \frac{d\omega}{\sqrt{2\pi}} e^{-i\omega t}\kappa(\omega)\int_{-\infty}^\infty d\tau e^{i\omega\tau}a_j(\tau), \tag{C4}$$

where $a_j(\tau) = e^{iH\tau}a_j e^{-iH\tau}$.

In order to calculate the evolution of $a_j(\tau)$, we assume coherent and low-power input signals. This allows us to write the evolution for a_j analogous to Eqs. (15),

$$\frac{d}{dt}\langle a_j\rangle = i\langle[H_{\rm eff}, a_{j,\lambda}]\rangle - i\sum_\lambda \left\langle A^{\rm in}_{j,\lambda}(t)\right\rangle + \frac{2}{\gamma}\langle D^\dagger[b_j]a_j\rangle + 2\kappa\langle D^\dagger[a_j]a_j\rangle. \quad \text{(C5)}$$

Compared to (15), the above expression includes an extra dissipation channel (always loss) due to the coupling to the feed lines, plus the driving due to the input signal. Without loss of generality, we can work with a monochromatic signal (any signal can be written in terms of monochromatic ones),

$$\left\langle A^{\rm in}_{1,L}(t)\right\rangle = \alpha\exp(i\omega_d t). \quad \text{(C6)}$$

Using linear response theory (LRT), we find

$$\langle a_j(\tau)\rangle = \chi_{a_j}^{A^{\rm in}}\exp(-i\omega_d t),$$
$$\chi_{a_j}^{A^{\rm in}} = \frac{1}{\alpha}\left[\Delta a_r(0) - i\omega\int_0^\infty dt\,\Delta a_r(t)\exp(-i\omega t)\right], \quad \text{(C7)}$$

where $\Delta a_r(t) = \langle a_j(t)\rangle - \langle a_j(t\to\infty)\rangle$ is the so-called relaxation response evolving with (15), without the drive. The initial condition $\langle a_j(0)\rangle$ is the equilibrium solution of (15) with a constant drive $\langle A^{\rm in}_{1R}(t)\rangle = \alpha$. This is the well-known LRT result where the ac response can be related to a dc relaxation experiment. With this result at hand, the calculation for $\langle a_j(\tau)\rangle$ is reduced to solving, in our case, a linear set of four coupled differential equations.

The RWA case

Here we will discuss some simplifications that can be used for computing $\langle a_j\rangle$ in the RWA case. The triumph of LRT is to avoid the time-dependent problem (15) in the ac response by using the formula in Eq. (C7). However, in the RWA case, we do not need to use this general formalism. The calculations are simpler by noting that we can work in a rotating basis with the drive ω_d [cf. Eq. (C6)]. In Eq. (C5), we have the terms a_j and $a^\dagger_{j'}$ appearing together. Thus, the equations are time independent with just a shift in the frequency, $\delta - \omega_d$. Introducing the notation

$$\alpha_j := \langle a_j\rangle, \quad \text{(C8)}$$

we can write

$$id_t\alpha_1 = (\delta-\omega_d)\alpha_1 + J\alpha_2 - i(\widetilde{\gamma}_1+\kappa)\alpha_1 - i\sqrt{\kappa}\left\langle A^{\rm in}_{1,L}\right\rangle,$$
$$id_t\alpha_2 = (\delta-\omega_d)\alpha_2 + J\alpha_1 + i(\widetilde{\gamma}_2-\kappa)\alpha_2. \quad \text{(C9)}$$

There is an analogous set for the complex conjugates. Let us, without loss of generality, consider the case where the input is sent through the port $1L$. Then, we have the following matrix form:

$$id_t\alpha = (M_{\rm RWA} - i\kappa\mathbb{I}_2)\alpha + \mathbf{j}, \quad \text{(C10)}$$

with

$$\mathbf{j} = -i\sqrt{\kappa}\begin{pmatrix}\left\langle A^{\rm in}_{1L}\right\rangle\\ 0\end{pmatrix}. \quad \text{(C11)}$$

In the rotating basis, the coherent input state (C6) is $\langle A^{\rm in}_{1L}\rangle = \alpha$. Then we find the response function,

$$\chi_{a_j}^{A^{\rm in}} = \alpha_j^{\rm eq}, \quad \text{(C12)}$$

with

$$\alpha_1^{\rm eq} = \frac{i\sqrt{\kappa}\alpha}{\omega_+\omega_-}[\delta + i(\widetilde{\gamma}_2-\kappa)], \quad \text{(C13)}$$
$$\alpha_2^{\rm eq} = -\frac{i\sqrt{\kappa}\alpha}{\omega_+\omega_-}J, \quad \text{(C14)}$$

where $\omega_\pm$ is given by

$$\omega_\pm = \delta + \tfrac{1}{2}[i(\widetilde{\gamma}_2 - \widetilde{\gamma}_1 - 2\kappa) \pm \sqrt{4J^2 - (\widetilde{\gamma}_1+\widetilde{\gamma}_2)^2}]. \quad \text{(C15)}$$

Then it is not difficult to solve the *input-output* relations in Eq. (27). For example, we can measure the transmitted signal in port $2L$ or $2R$, obtaining

$$\left\langle A^{\rm out}_{2R}\right\rangle = \frac{i\kappa\epsilon J}{\omega_+\omega_-}. \quad \text{(C16)}$$

[1] C. M. Bender and S. Boettcher, Real Spectra in Non-Hermitian Hamiltonians Having $\mathcal{PT}$ symmetry, Phys. Rev. Lett. **80**, 5243 (1998).

[2] C. M Bender, Introduction to $\mathcal{PT}$-symmetric quantum theory, Contemp. Phys. **46**, 277 (2005).

[3] C. E Rueter, K. G Makris, R. El-Ganainy, D. N Christodoulides, M. Segev, and D. Kip, Observation of parity-time symmetry in optics, Nat. Phys. **6**, 192 (2010).

[4] A. Guo, G. J. Salamo, D. Duchesne, R. Morandotti, M. Volatier-Ravat, V. Aimez, G. A. Siviloglou, and D. N. Christodoulides, Observation of $\mathcal{PT}$-Symmetry Breaking in Complex Optical Potentials, Phys. Rev. Lett. **103**, 093902 (2009).

[5] M. Brandstetter, M. Liertzer, C. Deutsch, P. Klang, J. Schöberl, H. E. Türeci, G. Strasser, K. Unterrainer, and S. Rotter, Reversing the pump dependence of a laser at an exceptional point, Nat. Commun. **5**, 4034 (2014).

[6] B. Peng, Ş. K. Özdemir, S. Rotter, H. Yilmaz, M. Liertzer, F. Monifi, C. M. Bender, F. Nori, and L. Yang, Loss-induced suppression and revival of lasing, Science **346**, 328 (2014).

[7] B. Peng, Ş. K. Özdemir, F. Lei, F. Monifi, M. Gianfreda, G. L. Long, S. Fan, F. Nori, C. M. Bender, and L. Yang, Parity-time-symmetric whispering-gallery microcavities, Nat. Phys. **10**, 394 (2014).

[8] A. Regensburger, C. Bersch, M.-A. Miri, G. Onishchukov, D. N. Christodoulides, and U. Peschel, Parity-time synthetic photonic lattices, Nature (London) **488**, 167 (2012).

[9] B. Peng, Ş. K Özdemir, M. Liertzer, W. Chen, J. Kramer, H. Yílmaz, J. Wiersig, S. Rotter, and L. Yang, Chiral modes and

directional lasing at exceptional points, Proc. Natl. Acad. Sci. USA **113**, 6845 (2016).
[10] P. Miao, Z. Zhang, J. Sun, W. Walasik, S. Longhi, N. M. Litchinitser, and L. Feng, Orbital angular momentum microlaser, Science **353**, 464 (2016).
[11] T. Gao, E. Estrecho, K. Y. Bliokh, T. C. H. Liew, M. D. Fraser, S. Brodbeck, M. Kamp, C. Schneider, S. Höfling, Y. Yamamoto, F. Nori, Y. S. Kivshar, A. G. Truscott, R. G. Dall, and E. A. Ostrovskaya, Observation of non-Hermitian degeneracies in a chaotic exciton-polariton billiard, Nature (London) **526**, 554 (2015).
[12] P. Peng, W. Cao, C. Shen, W. Qu, J. Wen, L. Jiang, and Y. Xiao, Anti-parity-time symmetry with flying atoms, Nat. Phys. **12**, 1139 (2016).
[13] R. Fleury, D. Sounas, and A. Alù, An invisible acoustic sensor based on parity-time symmetry, Nat. Commun. **6**, 5905 (2015).
[14] J. Schindler, A. Li, M. C. Zheng, F. M. Ellis, and T. Kottos, Experimental study of active lrc circuits with $\mathcal{PT}$ symmetries, Phys. Rev. A **84**, 040101 (2011).
[15] K.-H. Kim, M.-S. Hwang, H.-R. Kim, J.-H. Choi, Y.-S. No, and H.-G. Park, Direct observation of exceptional points in coupled photonic-crystal lasers with asymmetric optical gains, Nat. Commun. **7**, 13893 (2016).
[16] J. Doppler, A. A. Mailybaev, J. Böhm, U. Kuhl, A. Girschik, F. Libisch, T. J. Milburn, P. Rabl, N. Moiseyev, and S. Rotter, Dynamically encircling an exceptional point for asymmetric mode switching, Nature (London) **537**, 76 (2016).
[17] W. Chen, Ş. K. Özdemir, G. Zhao, J. Wiersig, and L. Yang, Exceptional points enhance sensing in an optical microcavity, Nature (London) **548**, 192 (2017).
[18] H. Hodaei, A. U. Hassan, S. Wittek, H. Garcia-Gracia, R. El-Ganainy, D. N. Christodoulides, and M. Khajavikhan, Enhanced sensitivity at higher-order exceptional points, Nature (London) **548**, 187 (2017).
[19] H. Xu, D. Mason, L. Jiang, and J. G. E. Harris, Topological energy transfer in an optomechanical system with exceptional points, Nature (London) **537**, 80 (2016).
[20] C. M. Bender, B. K. Berntson, D. Parker, and E. Samuel, Observation of $\mathcal{PT}$ phase transition in a simple mechanical system, Am. J. Phys. **81**, 173 (2013).
[21] S. Bittner, B. Dietz, U. Günther, H. L. Harney, M. Miski-Oglu, A. Richter, and F. Schäfer, $\mathcal{PT}$ Symmetry and Spontaneous Symmetry Breaking in a Microwave Billiard, Phys. Rev. Lett. **108**, 024101 (2012).
[22] N. M. Chtchelkatchev, A. A. Golubov, T. I. Baturina, and V. M. Vinokur, Stimulation of the Fluctuation Superconductivity by $\mathcal{PT}$ Symmetry, Phys. Rev. Lett. **109**, 150405 (2012).
[23] L. Feng, Z. J. Wong, R.-M. Ma, Y. Wang, and X. Zhang, Single-mode laser by parity-time symmetry breaking, Science **346**, 972 (2014).
[24] H. Hodaei, M.-A. Miri, M. Heinrich, D. N. Christodoulides, and M. Khajavikhan, Parity-time-symmetric microring lasers, Science **346**, 975 (2014).
[25] T. Eichelkraut, R. Heilmann, S. Weimann, S. Stützer, F. Dreisow, D. N. Christodoulides, S. Nolte, and A. Szameit, Mobility transition from ballistic to diffusive transport in non-Hermitian lattices, Nat. Commun. **4**, 2533 (2013).
[26] S. Longhi, D. Gatti, and G. D. Valle, Robust light transport in non-Hermitian photonic lattices, Sci. Rep. **5**, 13376 (2015).
[27] K. Kawabata, Y. Ashida, and M. Ueda, Information Retrieval and Criticality in Parity-Time-Symmetric Systems, Phys. Rev. Lett. **119**, 190401 (2017).
[28] Y. Ashida, S. Furukawa, and M. Ueda, Parity-time-symmetric quantum critical phenomena, Nat. Commun. **8**, 15791 (2017).
[29] B. Gardas, S. Deffner, and A. Saxena, $\mathcal{PT}$-symmetric slowing down of decoherence, Phys. Rev. A **94**, 040101 (2016).
[30] H. Jing, Ş. K. Özdemir, X.-Y. Lü, J. Zhang, L. Yang, and F. Nori, $\mathcal{PT}$-Symmetric Phonon Laser, Phys. Rev. Lett. **113**, 053604 (2014).
[31] H. Jing, Ş. K. Özdemir, Z. Geng, J. Zhang, X.-Y. Lü, B. Peng, L. Yang, and F. Nori, Optomechanically-induced transparency in parity-time-symmetric microresonators, Sci. Rep. **5**, 9663 (2015).
[32] H. Jing, Ş. K. Özdemir, H. Lü, and F. Nori, High-order exceptional points in optomechanics, Sci. Rep. **7**, 3386 (2017).
[33] H. Lü, Ş. K Özdemir, L.-M. Kuang, F. Nori, and H. Jing, Exceptional Points in Random-Defect Phonon Lasers, Phys. Rev. Appl. **8**, 044020 (2017).
[34] I. V. Barashenkov, D. A. Zezyulin, and V. V. Konotop, Jamming anomaly in pt-symmetric systems, New J. Phys. **18**, 075015 (2016).
[35] M. H. Devoret, Quantum fluctuations in electrical circuits, in *Quantum Fluctuations/Les Houches* (Elsevier, Amsterdam, Netherlands, 1997), pp. 351–386.
[36] J. Q. You and F. Nori, Quantum information processing with superconducting qubits in a microwave field, Phys. Rev. B **68**, 064509 (2003).
[37] A. Wallraff, D. I. Schuster, A. Blais, L. Frunzio, R.-S. Huang, J. Majer, S. Kumar, S. M. Girvin, and R. J. Schoelkopf, Strong coupling of a single photon to a superconducting qubit using circuit quantum electrodynamics, Nature (London) **431**, 162 (2004).
[38] J. Q. You and F. Nori, Superconducting circuits and quantum information, Phys. Today **58**, 42 (2005).
[39] J. Q. You and F. Nori, Atomic physics and quantum optics using superconducting circuits, Nature (London) **474**, 589 (2011).
[40] X. Gu, A. F. Kockum, A. Miranowicz, Y. xi Liu, and F. Nori, Microwave photonics with superconducting quantum circuits, Phys. Rep. **718-719**, 1 (2017).
[41] A. Baust, E. Hoffmann, M. Haeberlein, M. J. Schwarz, P. Eder, J. Goetz, F. Wulschner, E. Xie, L. Zhong, F. Quijandría, B. Peropadre, D. Zueco, J.-J. García Ripoll, E. Solano, K. Fedorov, E. P. Menzel, F. Deppe, A. Marx, and R. Gross, Tunable and switchable coupling between two superconducting resonators, Phys. Rev. B **91**, 014515 (2015).
[42] J. Q. You, Y.-xi Liu, C. P. Sun, and F. Nori, Persistent single-photon production by tunable on-chip micromaser with a superconducting quantum circuit, Phys. Rev. B **75**, 104516 (2007).
[43] J. Q. You, Y. xi Liu, and F. Nori, Simultaneous Cooling of An Artificial Atom and its Neighboring Quantum System, Phys. Rev. Lett. **100**, 047001 (2008).
[44] F. G. Paauw, A. Fedorov, C. J. P. M. Harmans, and J. E. Mooij, Tuning the Gap of a Superconducting Flux Qubit, Phys. Rev. Lett. **102**, 090501 (2009).
[45] M. J. Schwarz, J. Goetz, Z. Jiang, T. Niemczyk, F. Deppe, A. Marx, and R. Gross, Gradiometric flux qubits with a tunable gap, New J. Phys. **15**, 045001 (2013).

[46] J. Q. You, X. Hu, S. Ashhab, and F. Nori, Low-decoherence flux qubit, Phys. Rev. B **75**, 140515 (2007).

[47] J. Koch, T. M. Yu, J. Gambetta, A. A. Houck, D. I. Schuster, J. Majer, A. Blais, M. H. Devoret, S. M. Girvin, and R. J. Schoelkopf, Charge-insensitive qubit design derived from the Cooper pair box, Phys. Rev. A **76**, 042319 (2007).

[48] A. Baust, E. Hoffmann, M. Haeberlein, M. J. Schwarz, P. Eder, J. Goetz, F. Wulschner, E. Xie, L. Zhong, F. Quijandría, D. Zueco, J.-J. Garcia Ripoll, L. García-Álvarez, G. Romero, E. Solano, K. G. Fedorov, E. P. Menzel, F. Deppe, A. Marx, and R. Gross, Ultrastrong coupling in two-resonator circuit qed, Phys. Rev. B **93**, 214501 (2016).

[49] D. Underwood, W. Shanks, J. Koch, and A. Houck, Low-disorder microwave cavity lattices for quantum simulation with photons, Phys. Rev. A **86**, 023837 (2012).

[50] B. Peropadre, D. Zueco, F. Wulschner, F. Deppe, A. Marx, R. Gross, and J. J. García-Ripoll, Tunable coupling engineering between superconducting resonators: From sidebands to effective gauge fields, Phys. Rev. B **87**, 134504 (2013).

[51] S. Felicetti, M. Sanz, L. Lamata, G. Romero, G. Johansson, P. Delsing, and E. Solano, Dynamical Casimir Effect Entangles Artificial Atoms, Phys. Rev. Lett. **113**, 093602 (2014).

[52] J. I. Cirac, R. Blatt, P. Zoller, and W. D. Phillips, Laser cooling of trapped ions in a standing wave, Phys. Rev. A **46**, 2668 (1992).

[53] F. Quijandría, D. Porras, J. J. García-Ripoll, and D. Zueco, Circuit QED Bright Source for Chiral Entangled Light Based on Dissipation, Phys. Rev. Lett. **111**, 073602 (2013).

[54] F. Quijandría, U. Naether, D. Porras, J. J. García-Ripoll, and D. Zueco, The bose–hubbard model with squeezed dissipation, J. Phys. B **48**, 055302 (2015).

[55] B. Peng, Ş. K. Özdemir, W. Chen, F. Nori, and L. Yang, What is and what is not electromagnetically induced transparency in whispering-gallery microcavities, Nat. Commun. **5**, 5082 (2014).

[56] C. W. Gardiner and M. J. Collett, Input and output in damped quantum systems: Quantum stochastic differential equations and the master equation, Phys. Rev. A **31**, 3761 (1985).

[57] U. Naether, J. J. García-Ripoll, J. J. Mazo, and D. Zueco, Quantum Chaos in an Ultrastrongly Coupled Bosonic Junction, Phys. Rev. Lett. **112**, 074101 (2014).

[58] S. Ashhab, J. R. Johansson, A. M. Zagoskin, and Franco Nori, Two-level systems driven by large-amplitude fields, Phys. Rev. A **75**, 063414 (2007).

[59] D. Zueco, G. M. Reuther, S. Kohler, and P. Hänggi, Qubit-oscillator dynamics in the dispersive regime: Analytical theory beyond the rotating-wave approximation, Phys. Rev. A **80**, 033846 (2009).

[60] J. Casanova, G. Romero, I. Lizuain, J. J. García-Ripoll, and E. Solano, Deep Strong Coupling Regime of the Jaynes-Cummings Model, Phys. Rev. Lett. **105**, 263603 (2010).

[61] L. Garziano, R. Stassi, V. Macrì, A. F. Kockum, S. Savasta, and F. Nori, Multiphoton quantum Rabi oscillations in ultrastrong cavity qed, Phys. Rev. A **92**, 063830 (2015).

[62] Á. Rivas and S. F. Huelga, *Open Quantum Systems*, Springer Briefs in Physics (Springer Berlin, Heidelberg, 2011), p. 100.